WARSAW UNIVERSITY OF TECHNOLOGY Index 351733
FACULTY OF CIVIL ENGINEERING
COMMITTEE FOR CIVIL AND WATER ENGINEERING
POLISH ACADEMY OF SCIENCES ISSN 1230-2945

DOI: 10.24425/ace.2023.146075

ARCHIVES OF CIVIL ENGINEERING

Vol. LXIX ISSUE 3 2023

pp. 187 –197

Research paper

On the resistance of concrete hollow thin-walled high piers to rock collisions

Yao Huang[1]

Abstract: Concrete hollow thin-walled high piers (CHTWHPs) located in mountainous areas may be destroyed by the huge impact force of accidental rocks. The study focuses on analyzing the effects of rock impact on the pier, including its impact force, pier damage, dynamic response, and energy dissipation characteristics. The results show that: (1) Increasing the impact height led to a decrease in the peak impact force. Specifically, 15.5% decrease in the peak collision force is induced when the height of rock collision rises from 10 m to 40 m. (2) The damage mode of the pier's collision surface is mainly oval damage with symmetrical center, radial damage on the side surface, and corner shear failure on the cross section. (3) The peak displacement of bridge pier increases with the increase of collision height. As the collision height increased from 10 m to 40 m, the bridge pier's peak displacement also increased, rising by 104.2%. (4) The concrete internal energy gradually decreased with increasing collision height, dropping by 36.9% when the height of rock collision rises from 10 m to 40 m. The reinforcement internal energy showed an increase of 78%. The results of this study may provide reference for the rock collision resistance design of CHTWHPs.

Keywords: concrete hollow thin-walled high pier, rock collision, collision force, pier damage, collision resistance

[1]MSc., Eng., Nanning College of Technology, Guangxi, 541006, China, e-mail: huangyao_2022@163.com, ORCID: 0000-0001-6960-1822

1. Introduction

China's mountainous topography has resulted in a rise in the construction of large bridges spanning valleys, thanks to the ongoing enhancements in transportation infrastructure [1]. However, due to the intricate terrain and extreme weather, these bridges often encounter risks such as rockslides caused by downpours, earthquakes, and mudslides, and it is not unusual for them to be hit by rocks. For example, after the completion of the Cheheyan Bridge in China, due to the combined effects of an earthquake and heavy rain, the bridge piers were again broken by falling rocks, causing the bridge to collapse. This not only resulted in the interruption of National Highway 213, but also caused vehicles and personnel on the bridge to fall into the river, resulting in 3 deaths, 12 injuries, and 7 damaged vehicles. In addition, a 1.6-kilometer section of the Baocheng Railway was hit by falling rocks 46 times in just 20 years (1961–1981), causing rail damage and train shutdowns [2]. Continuous beam bridges, as an key transportation structure for spanning canyons, generally use concrete hollow thin-walled piers to save materials and reduce costs. Concrete hollow thin-walled piers located in mountainous areas may be damaged due to the huge collision force caused by accidental falling rocks.

Few researchers conducted full sized model tests to examine the collision resistance of column-like structures. Consolazio et al. [3] employed a full sized model test and numerical analysis to evaluate the pier response, collision load, and soil response of bridge piers during barge collisions. Buth et al. [4] performed two tests between an 80000-pound heavy-duty truck-style tractor-trailer and a full-scale bridge pier, one in a head-on configuration and the other with an eccentric distance between the vehicle and the pier, at a speed of 80 km/h. Xiao et al. [5] executed vehicle collision tests with an actual car to investigate the anti-collision performance of a steel-concrete anti-collision column system. Researchers are more inclined to utilize numerical simulations over full-sized tests when studying the collision performance of piers [6–12]. In addition, researchers also studied the resistance of bridge piers under rock collision using numerical simulation [13–17]. However, these studies mainly focused on solid concrete section bridge piers, and no scholars have yet focused on the resistance of concrete hollow thin-walled high piers under rock collision.

The present study employs ANSYS/LS-DYNA to create a model of a CHTWHP subjected to rock. The model is validated by drop hammer testing, following which the collision force, damage, dynamic response, and energy dissipation properties of the CHTWHP under rockfall are investigated. This analysis offers valuable insights into the design of the pier's performance under rock collision.

2. CHTWHP-rock model

2.1. Model establishment

This article focuses on a four-span rigid-frame bridge in Hunan, China, a mountainous region where rockfall accidents usually happen, with a maximum span 120 m. The bridge's main beam has a single-box, single-chamber cross-section, and its height con-

forms to a second-order parabolic curve. The bridge piers are typical hollow thin-walled pier structures, with a central pier height of 100 m and side pier height of 80 m. The diagram of the bridge is presented in Fig. 1. The CHTWHPs have a narrow top and wide bottom, with a rectangular outer contour of 5×3 m at the top and 7.5×4 m at the bottom. The thickness of the section is 0.5 m. The gravity is considered by using the keyword *Load_body_z. The falling rock is simulated as a sphere, and the material is modeled as a rigid body (*MAT_RIGID) [6], with a diameter and initial velocity set at 1.5 m and 20 m/s, respectively. The continuous surface cap model (CSCM) model is selected to simulate the dynamic performance and damage characteristics of concrete under collision. The concrete grade is C30, and the CSCM material model parameters are generated by the model's automatic algorithm. The failure of concrete is considered by using the keyword *MAT_ADD_EROSION. The longitudinal and hoop reinforcement are modelled by the *MAT_PLASTIC_KINEMATIC model. The relationship between steel and concrete is assumed to be completely bonded, and the CONSTRAINED_LAGRANGE_IN_SOLID keyword is used to implement it. The values of the failure strains for the longitudinal and hoop reinforcement are 0.25 and 0.20, respectively [6]. The material parameters for the longitudinal and transverse rebars are shown in Table 1. Fig. 2 shows the finite element model. Fig. 3 further shows the detailed view of the CHTWHP.

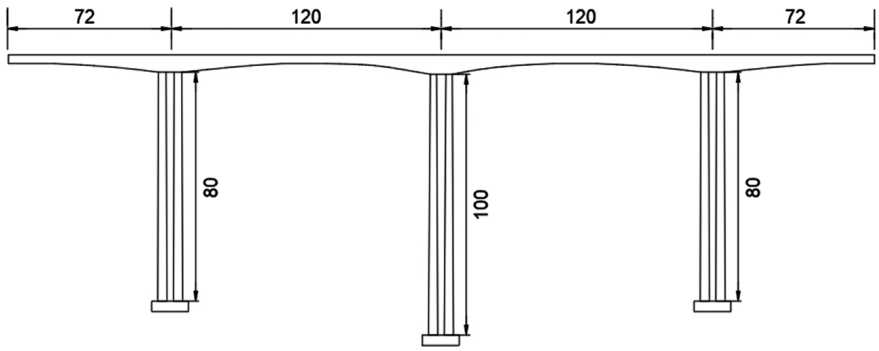

Fig. 1. Dimensions of the bridge (unit: m)

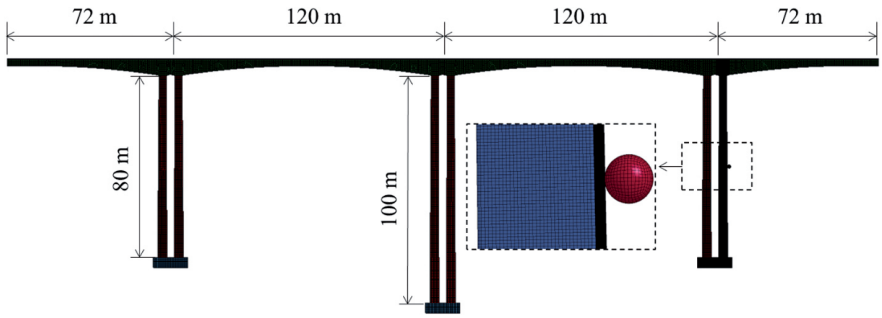

Fig. 2. The CHTWHP-rock model

Table 1. Parameters for material models of the reinforcement

Steel bars	Material model	Parameter	Value
Concrete	*MAT_159	Density (g/cm^3)	2.4
		Elasticity modulus (GPa)	27.8
		Poisson's ratio	0.2
Transverse	*MAT_PLASTIC_KINEMATIC	Elasticity modulus (GPa)	210
		Density (g/cm^3)	7.85
		Poisson's ratio	0.3
		Failure strain	0.25
		Yield strength (MPa)	300
Longitudinal	*MAT_PLASTIC_KINEMATIC	Elasticity modulus (GPa)	210
		Density (g/cm^3)	7.85
		Poisson's ratio	0.3
		Failure strain	0.2
		Yield strength (MPa)	400

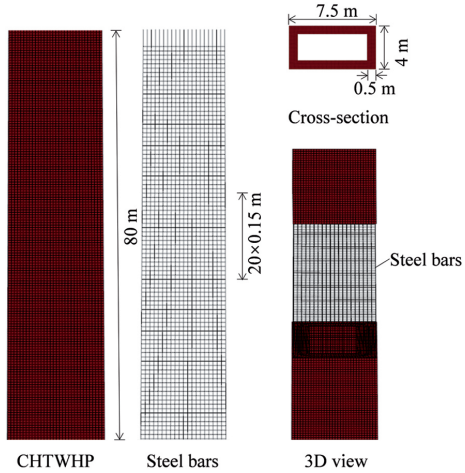

Fig. 3. Detailed view of the CHTWHP

2.2. Model validation

The material model and contact algorithm used in this study were verified by Fujikake et al.'s [18] collision tests on reinforced concrete beams. The height of the steel hammer is 400 kg and the concrete uniaxial compressive strength of concrete is 42 MPa. The beam has a rectangular cross-section of 150×250 mm and a length of 1700 mm. A condition with longitudinal steel bars of 16 mm diameter and a reinforcement ratio of 1.26% was selected for

validation, with corresponding collision heights of 0.15 m, 0.3 m, 0.6 m, and 1.2 m. Fig. 4 shows the comparison of the test and finite element damage for different collision heights, and Table 2 compares of the maximum contact force and mid-span deflection. As shown in Fig. 4, in all collision height conditions, the concrete beams in the test and finite element model exhibited similar overall bending damage, with several flexural cracks appearing on the underside of the beams. As shown in Table 2, the maximum error in peak collision force and mid-span displacement peak was 2.8%. This analysis demonstrates that the material model and collision algorithm used in this study can accurately simulate the dynamic response and damage of concrete structures with reinforcements under collision loads.

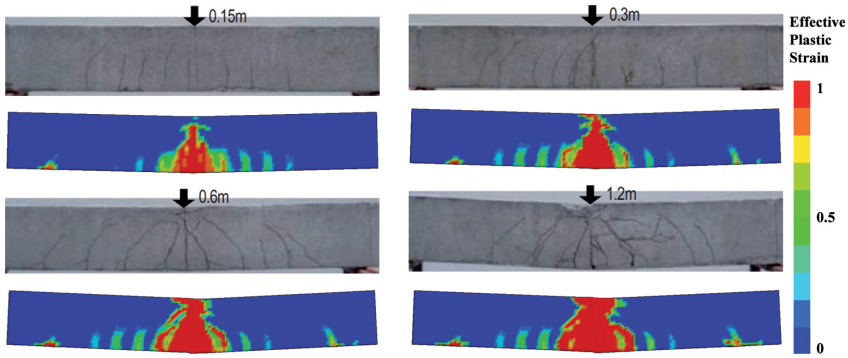

Fig. 4. Comparison of damage

Table 2. Comparison of mid-span deflection and maximum contact force

Collision height	Mid-span deflection/mm			Maximum contact force/kN		
	Experiment	Numerical model	Difference	Experiment	Numerical model	Difference
0.15 m	6.1	6.2	1.6%	124.3	125.8	1.2%
0.30 m	10.9	10.6	2.8%	182.7	180.9	1.0%
0.60 m	20	20.2	1.0%	243.8	250.7	2.8%
1.20 m	36.6	36.5	0.3%	308.4	310.9	0.8%

3. Results

3.1. Contact force

According to the investigation of rock disasters in western mountainous areas of China, the collision of rock on bridge piers generally occurs in the middle and lower parts of the pier. Therefore, the rock collision heights h are taken as 10, 20, 30, and 40 m, respectively. Fig. 5 shows the time-history curves of the collision force under different heights of rock collision.

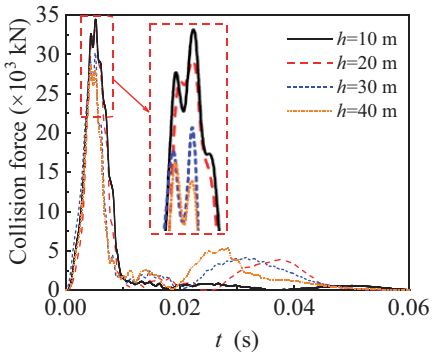

Fig. 5. Collision force

At t = 0 s, the rock collides with the pier, causing an instantaneous and rapidly rising collision force that peaks within 0.005 s. This instantaneous contact results in a local acceleration of the concrete and a deceleration of the rock. Then, the rock and the pier detach from contact, so the collision force rapidly decreases after reaching the peak. The inherent elasticity and plasticity of the pier cause it to vibrate, resulting in a fluctuation in the subsequent collision force time-history curve. Additionally, the peak collision force reduces as the collision position increases, with a decrease of 15.5% observed from 10 m to 40 m. This phenomenon is due to the pier being subjected to a stronger constraint when closer to the pier bottom, resulting in a larger corresponding peak collision force.

3.2. Damage of CHTWHP

Fig. 6 shows the damage evolution on the collision face and side of CHTWHP when the collision height is 40 meters. As shown in Fig. 6a, when a CHTWHP is collided by falling rocks, an elliptical damage area appears on the collision face with the rock as the center, and the damage degree deepens with time and spreads vertically and towards the

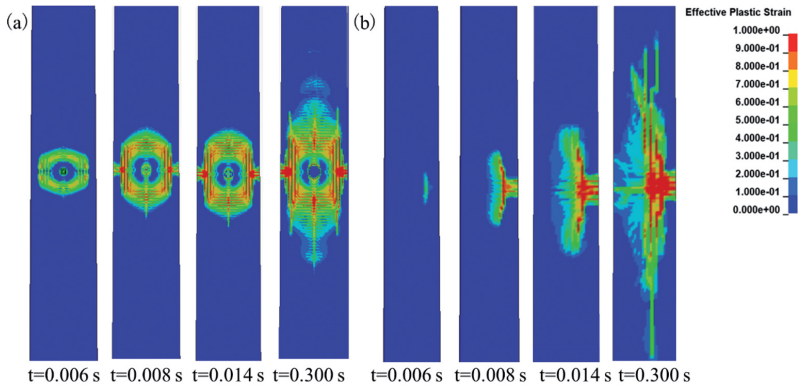

Fig. 6. Damage evolution (h = 40 m): (a) collision face; (b) side face

pier edge. As shown in Fig. 6b, a triangular compressed damage region appears on the side of CHTWHP near the collision face position, and this triangular damage area continues to expand towards the back of the pier and vertically along the pier. The damage degree to the pier intensifies over time, eventually developing to a radial damage region that penetrates the side of the pier. Fig. 7 shows the damage evolution of the cross-section when the rock collides at 40 m. When a CHTWHP is impacted by falling rocks, the inside of the pier is under tension, so the damage degree on the inside is severer than on the outside. As the collision process progresses, the cross-sectional damage expands from local to the entire collision face, and the damage at the corner of the collision face is particularly severe. Two slender shear damage regions appear at the back corner of the pier, and they are symmetrically distributed.

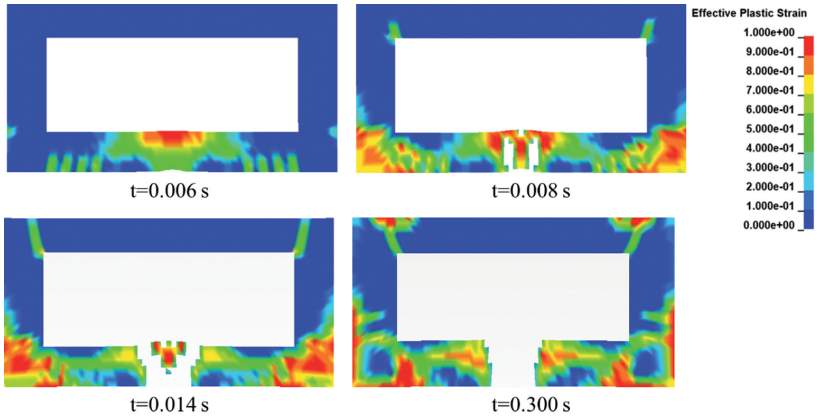

Fig. 7. Damage evolution of the cross-section (h = 40 m)

Fig. 8 displays the damage of the pier's collision face and side under different collision height conditions. Fig. 8a illustrates that the pier's collision face primarily experiences centrally symmetric elliptical damage under various collision heights, with a relatively similar degree of damage. Conversely, Fig. 8b shows a radial damage area that pierces through the pier's side under different collision height conditions, with no significant

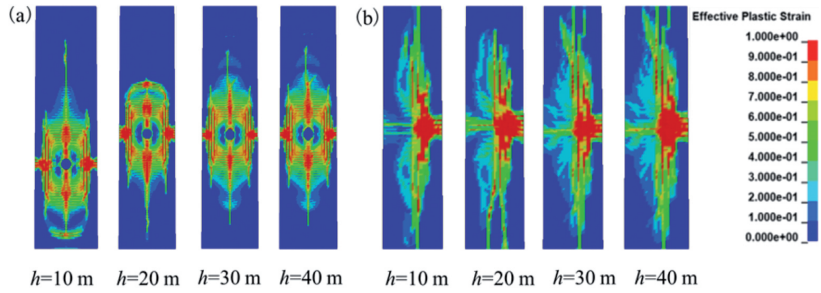

Fig. 8. Influence of collision height on damage: (a) collision face; (b) side face

difference in the area and degree of damage. Fig. 9 presents the damage on the pier's cross-section under various collision height conditions. The figure reveals that as the falling rock collision position moves upwards, the degree of cross-sectional damage and the damage area remain relatively similar, with shear damage at the corner being the primary mode of destruction. These observations suggest that the collision of the falling rock's height on pier damage is limited, possibly because the initial collision velocity of the falling rock is consistent in all four conditions, resulting in similar kinetic energy and damage to the pier.

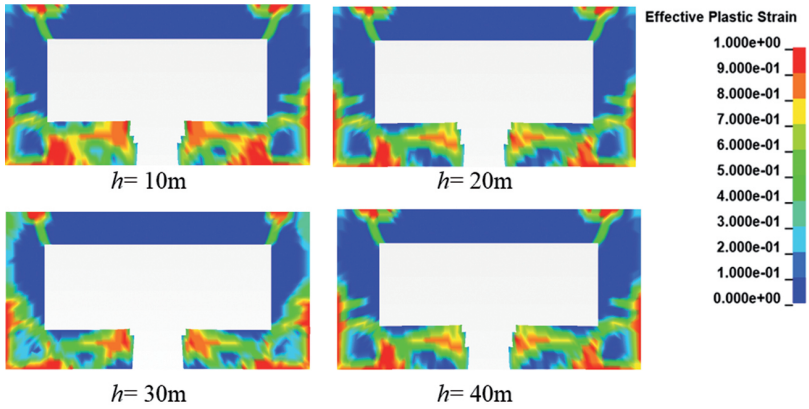

Fig. 9. Influence of collision height on cross-sectional damage

3.3. Dynamic response of the CHTWHP

Figs. 10 and 11 show the displacement-time and peak displacement characteristics of the CHTWHP subjected to rock collision at different heights. As shown in Fig. 10, the cross-section at the collision location (40 m) experiences the first increase in displacement, followed by the sections above and below it due to the propagation of stress waves. The initial displacement growth rates of the sections at 30 m and 50 m, 20 m and 60 m, 10 m and 70 m are similar.

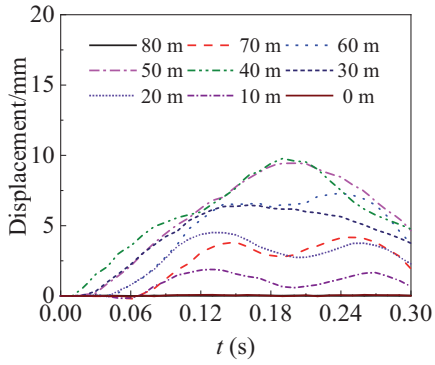

Fig. 10. Displacement curves (h = 40 m)

The collision point experiences the highest peak displacement of 9.77 mm across all sections, with significantly lower displacements observed at the top and bottom sections of the pier due to constraints. The peak displacement of the cross-sections above the collision point occurs later than the cross-sections below due to the upper part of the pier's increased flexibility and deformability.

Fig. 11 shows the peak displacement of different pier sections for different collision heights. The peak displacement of all four scenarios occurs in the range of 40-60 m height, where the lower section has lager stiffness and deformation resistance. As the collision height increases, the peak displacement also increases. The peak displacement increases by 104.2% as the collision height rises from 10 m to 40 m, because the pier sections become weaker as the collision point gets closer to the pier top.

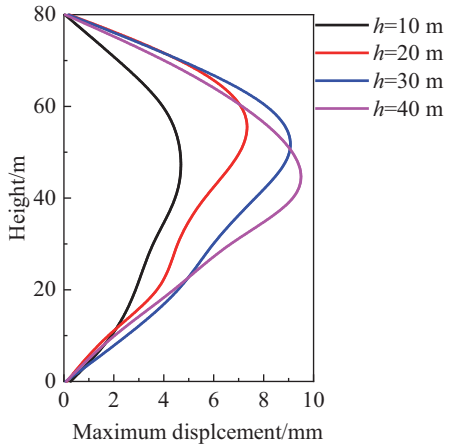

Fig. 11. Influence of collision height on the displacement response

3.4. Energy dissipation

Fig. 12 shows the energy dissipation of different materials at different collision heights. During the collision process, most of the kinetic energy of the falling rock gradually converts into the internal energy of the steel bars and concrete. Meanwhile, a small fraction of kinetic energy is dissipated in the form of heat energy. As the collision height increases, the internal energy of concrete gradually decreases. When the collision height rises from 10 m to 40 m, the decrease in internal energy of concrete is 36.9%, while the internal energy of steel bars keeps increasing, with an increase of 78%. At the same time, the kinetic energy of concrete and steel bars remains almost constant, and the energy dissipation values are low, about 0.003×106 J. Since the total kinetic energy of the falling rock remains unchanged, the total energy dissipation of the bridge pier is almost equal. As the strain energy of the steel bars is much higher than that of the concrete, when the collision height increases, the deformation of the CHTWHP increases, leading to a gradual shift in the main energy dissipation material of the CHTWHP from concrete to steel bars.

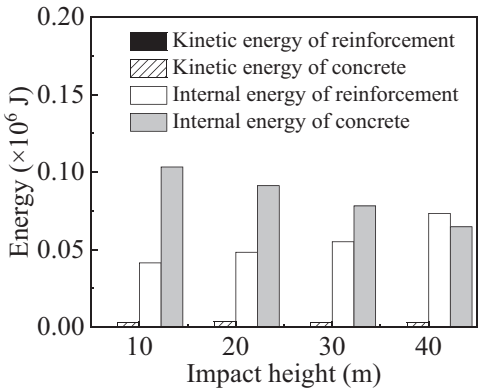

Fig. 12. Influence of collision height on energy dissipation

4. Conclusions

This article established a collision model of falling rocks and hollow thin-walled piers based on ANSYS/LS-DYNA dynamic analysis software and studied the anti-collision performance of hollow thin-walled piers under falling rock collision. Some conclusions are:

1. Increasing the impact height led to a decrease in the peak impact force. Specifically, 15.5% decrease in the peak collision force is induced when the height of rock collision rises from 10 m to 40 m.
2. The damage mode of the pier's collision surface is mainly oval damage with symmetrical center, radial damage on the side surface, and corner shear failure on the cross-section.
3. The peak displacement of bridge pier increases with the increase of collision height. As the collision height increased from 10 m to 40 m, the bridge pier's peak displacement also increased, rising by 104.2%.
4. The concrete internal energy gradually decreased with increasing collision height, dropping by 36.9% when the height of rock collision rises from 10 m to 40 m. The reinforcement internal energy showed an increase of 78%.

Despite the analysis conducted in this research, we are not able to perform a corresponding experiment at our current ability. An impact experiment of rock-bridge pier will be carried out in the future for verifying the simulation program.

References

[1] W.C. Yang, Y.K. Liu, E. Deng, Y.W. Wang, X.H. He, and M.F. Lei, "Characteristics of wind field at tunnel-bridge area in steep valley: Field measurement and LES study", *Measurement*, vol. 202, art. no. 111806, 2022, doi: 10.1016/j.measurement.2022.111806.

[2] X. Zhang, X. Wang, W. Chen, Z. Wen, and X. Li, "Numerical study of rockfall impact on bridge piers and its effect on the safe operation of high-speed trains", *Structure and Infrastructure Engineering*, vol. 17, no. 1, pp. 1–19, 2021, doi: 10.1080/15732479.2020.1730406.

[3] G.R. Consolazio, R.A. Cook, M.C. McVay, D. Cowan, A. Biggs, and L. Bui, *Barge impact testing of the St. George Island Causeway Bridge, Phase III: physical testing and data interpretation*. University of Florida, 2006.

[4] C.E. Buth, M.S. Brackin, W.F. Williams, and G.T. Fry, *Collision loads on bridge piers: phase 2, report of guidelines for designing bridge piers and abutments for vehicle collisions*. Texas Transportation Institute, 2011.

[5] Y. Xiao, L. Chen, X. Guo, B.S. Chen, and C.L. Chun, "Tests for anti-ram bollards based on truck collision", *Journal of Vibration and Shock*, vol. 32, no. 11, pp. 1–6, 2013, doi: 10.13465/j.cnki.jvs.2013.11.028.

[6] Y.K. Liu, J. Yang, G.J. Xu, H. Wei, and E. Deng, "Performance of UHPC bridge piers subjected to heavy vehicle collisions and probability analysis of damage level", *Structures*, vol. 47, pp. 212–232, 2023, doi: 10.1016/j.istruc.2022.11.061.

[7] W. Fan, B. Liu, and G.R. Consolazio, "Residual capacity of axially loaded circular RC columns after lateral low-velocity impact", *Journal of Structural Engineering*, vol. 145, no. 6, 2019, doi: 10.1061/(asce)st.1943-541x.0002324.

[8] L. Buda-Ożóg, J. Zięba, K. Sieńkowska, and D. Nykiel, "Influence of the tie reinforcement on the development of a collapse caused by the failure of an edge column in RC flat slab system", *Archives of Civil Engineering*, vol. 69, no. 1, pp. 39–54, 2023, doi: 10.24425/ace.2023.144158.

[9] Y. Shi, H. Hao, and Z.-X. Li, "Numerical derivation of pressure-impulse diagrams for prediction of RC column damage to blast loads", *International Journal of Impact Engineering*, vol. 35, no. 11, pp. 1213–1227, 2008, doi: 10.1016/j.ijimpeng.2007.09.001.

[10] D. Bertrand, F. Kassem, F. Delhomme, and A. Limam, "Reliability analysis of an RC member impacted by a rockfall using a nonlinear SDOF model", *Engineering Structures*, vol. 89, pp. 93–102, 2015, doi: 10.1016/j.engstruct.2015.01.051.

[11] Y. Yu, L. Deng, W. Wang, and C.S. Cai, "Local impact analysis for deck slabs of prestressed concrete box-girder bridges subject to vehicle loading", *Journal of Vibration and Control*, vol. 23, no. 1, pp. 31–45, 2017, doi: 10.1177/1077546315575434.

[12] A. Ventura, V. De Biagi, and B. Chiaia, "Effects of rockfall on an elastic-plastic member: A novel compliance contact model and dynamic response", *Engineering Structures*, vol. 148, pp. 126–144, 2017, doi: 10.1016/j.engstruct.2017.06.046.

[13] R. Xie, W. Fan, B. Liu, and D. Shen, "Dynamic behavior and vulnerability analysis of bridge columns with different cross-sectional shapes under rockfall impacts", *Structures*, vol. 26, pp. 471–486, 2020, doi: 10.1016/j.istruc.2020.04.042.

[14] W.C. Yang, Y.K. Liu, E. Deng, X.H. He, M.F. Lei, and Y.F. Zou, "Comparative study on the wind characteristics of tunnel–bridge and tunnel–flat ground infrastructures on high-speed railway", *Journal of Wind Engineering and Industrial Aerodynamics*, vol. 226, art. no. 105006, 2022, doi: 10.1016/j.jweia.2022.105006.

[15] M. Kiraga, S. Bajkowski, and J. Urbański, "Bridge headwater afflux estimation using bootstrap resampling method", *Archives of Civil Engineering*, vol. 69, no. 1, pp. 21–37, 2023, doi: 10.24425/ace.2023.144157.

[16] F. Li, Y.K. Liu, and J. Yang, "Durability assessment method of hollow thin-walled bridge piers under rockfall impact based on damage response surface", *Sustainability*, vol. 14, no. 19, art. no. 12196, 2022, doi: 10.3390/su141912196.

[17] V.D. Tin, M.P. Thong, and H. Hao, "Proposed design procedure for reinforced concrete bridge columns subjected to vehicle collisions", *Structures*, vol. 22, pp. 213–229, 2019, doi: 10.1016/j.istruc.2019.08.011.

[18] K. Fujikake, B. Li, and S. Soeun, "Impact response of reinforced concrete beam and its analytical evaluation", *Journal of Structural Engineering*, vol. 135, no. 8, pp. 938–950, 2009, doi: 10.1061/(asce)st.1943-541x.0000039.

Received: 2023-03-27, Revised: 2023-04-20